THE UNIVERSITY OF TEXAS AT SAN ANTONIO, COLLEGE OF BUSINESS

Working Paper SERIES

Date May 11, 2010

WP # 0011MSS-KEYINGYE-2010

Sea ice thickness distribution of the Bellingshausen Sea from surface measurements and ICESat altimetry

H. Xie
Department of Geological Sciences,
University of Texas at San Antonio, Texas 78249, USA

S.F. Ackley
Department of Geological Sciences,
University of Texas at San Antonio, Texas 78249, USA

D. Yi
Goddard Space Flight Center,
Greenbelt, MD 20771, USA

H.J. Zwally
Goddard Space Flight Center,
Greenbelt, MD 20771, USA

P. Wagner
Department of Geological Sciences,
University of Texas at San Antonio, Texas 78249, USA

B. Weissling
Department of Geological Sciences,
University of Texas at San Antonio, Texas 78249, USA

M. Lewis
Department of Geological Sciences,
University of Texas at San Antonio, Texas 78249, USA

K. Ye
Department of Management Science and Statistics
University of Texas at San Antonio, Texas 78249, USA

UTSA COLLEGE OF BUSINESS KNOWLEDGE FOR A NEW WORLD

ONE UTSA CIRCLE
SAN ANTONIO, TEXAS 78249-0631
210 458-4317 | BUSINESS.UTSA.EDU

Sea ice thickness distribution of the Bellingshausen Sea from surface measurements and ICESat altimetry

H. Xie[1], S.F. Ackley[1], D. Yi[2], H.J. Zwally[3], P. Wagner[1*], B. Weissling[1], M. Lewis[1], K. Ye[4]

[1]Laboratory for Remote Sensing and Geoinformatics, Department of Geological Sciences, University of Texas at San Antonio, Texas 78249, USA

[2]SGT Inc., Cryospheric Sciences Branch, Code 614.1, Goddard Space Flight Center, Greenbelt, MD 20771, USA

[3]Cryospheric Sciences Branch, Code 614.1, Goddard Space Flight Center, Greenbelt, MD 20771, USA

[4]Department of Management Science and Statistics, University of Texas at San Antonio, Texas, 78249, USA

[*]Now at Dept. of Geography, Univ. of Delaware, Newark, DE, USA

Abstract

Although sea ice extent in the Bellingshausen-Amundsen (BA) seas sector of the Antarctic has shown significant decline over several decades, there is not enough data to draw any conclusion on sea ice thickness and its change for the BA sector, or for the entire Southern Ocean. This paper first presents our results of snow and ice thickness distributions from the SIMBA 2007 experiment in the Bellingshausen Sea, using four different methods (ASPeCt ship observations, downward-looking camera imaging, ship-based electromagnetic induction (EM) sounding, and *in situ* measurements using ice drills). A snow freeboard and ice thickness model generated from *in situ* measurements was then applied to contemporaneous ICESat (satellite laser altimetry) measured freeboard to derive ice thickness at the ICESat footprint scale. Errors from *in situ* measurements and from ICESat freeboard estimations were incorporated into the model, so a thorough evaluation of the model and uncertainty of the ice thickness estimation from ICESat are possible. Our results indicate that ICESat derived snow freeboard and ice thickness distributions (asymmetrical unimodal tailing to right) for first year ice (0.29±0.14 m for mean snow freeboard and 1.06±0.40 m for mean ice thickness), multi-year ice (0.48±0.26m and 1.59±0.75m, respectively), and all ice together (0.42±0.24m and 1.38±0.70m, respectively) for the study area seem reasonable compared with those values from the *in situ* measurements, ASPeCt observations, and EM measurements. The EM measurements can act as an appropriate supplement for ASPeCt observations taken hourly from the ship's bridge and provide reasonable ice and snow distributions under homogeneous ice conditions. Our proposed approaches: (1) of using empirical equations relating snow freeboard to ice thickness based on *in situ* measurements and (2) of using isostatic equations that replace snow depth with snow freeboard (or empirical equations that convert freeboard to snow depth), are efficient and important ways to derive ice thickness from ICESat altimetry at the footprint scale for Antarctic sea ice. Spatial and temporal snow and ice thickness from satellite altimetry for the BA sector and for the entire Southern Ocean is therefore possible.

Keywords: ASPeCt, Electromagnetic induction, ICESat, sea ice thickness, Antarctic sea ice
JEL Code: C11, C13,

1. Introduction

In overall behavior, sea ice in the Antarctic has shown a slight increasing extent trend (~1%/decade) during the satellite era (1979-2008) (Comiso and Nishio, 2008). The Bellingshausen-Amundsen (BA) region and the Ross Sea region, however, have shown contrasting trends, with the BA region declining overall, by -5.7% /decade, while the Ross Sea region has increased by +4.2% /decade (Comiso and Nishio, 2008). The Ross Sea gains have exceeded the BA's losses by 50% in absolute area and have amounted to over half the gain seen for the Antarctic region as a whole (Comiso and Nishio, 2008). While the rough picture of sea ice extent and trend of change have been generalized by satellite images, "there are insufficient data to draw any conclusions about trends in the Antarctic sea ice thickness and snow cover over sea ice" (IPCC-C4, 2007). For the Arctic, decades of under-ice submarine traverses using upward-looking sonar and modeling have shown a significant thickness decrease since the late 1980s (Tucker et al., 2001; Rothrock et al., 1999, 2003; Wadhams and Davis, 2000; Stroeve et al., 2007, 2008). In the Antarctic sea ice zone, however, there is no large-scale program of submarine observations. Satellite-based radar altimetry (ERS 1 and 2, ENVISat, and Cryosat-2 in 2010) and laser altimetry (ICESat) have provided reasonable sea ice thickness estimates for the Arctic region and match well with other observations (Kwok et al., 2004, 2007; Giles et al., 2007, 2008; Kwok and Cunningham, 2008). For the Antarctic, however, more complex sea ice and snow conditions exist, with negative ice freeboards and snow/ice interface flooding causing slush layers, as illustrated in Figure 1. In the context of the buoyancy, this creates a more complex geometry, alternating between two and three layer systems across any given ice floe. Algorithms for deriving sea ice thickness from radar/laser altimetry using buoyancy theory in considering those different situations are still under development and validation (Giles, et al., 2008b). Another difficult task for estimating ice thickness from altimetry using buoyancy theory is the estimation of snow depth (Kurtz et al. 2009). Many studies used either the AMSR-E snow depth, derived from passive microwave satellite imagery (Markus and Cavalieri, 1998), or snow climatology (Kurtz et al. 2009; Zwally et al., 2008, Kwok et al., 2007). Both are prone to considerable uncertainty (error) in the estimation of ice thickness. To make things even more difficult for Antarctic sea ice, however, there is no good climatology-based snow depth information available. The AMSR-E snow depth products are not well validated over Antarctic sea ice. The 50 cm snow depth limitation based on the passive microwave frequencies used in the current AMSR-E algorithm (Markus et al. 1998; Comiso et al. 2003; Powell et al., 2006) is another issue, since the snow depth over Antarctic sea ice can be well over 60 cm in some regions (Weissling et al., Lewis, et al., this issue). Consequently, ship-based ice observations based on the ASPeCt (Antarctic Sea Ice Processes and Climate) protocol (Worby and Allison, 1999) were, and still are, the most important means to provide sea ice thickness and snow cover information for the Antarctic sea ice zone (Worby et al. 2008).

Due to limited access (primarily related to the ice breaking capability of research vessels), the Antarctic sea ice region, particularly the BA sector, represents the least studied sea ice region in the world's oceans. Worby et al. (2008), for example, have shown from 81 sets of ship-based sea ice observations (ASPeCt), where ice thicknesses and snow depths were estimated over the circumpolar Antarctic sea ice zone, that the largest data gaps are in the BA sector in all seasons. Worby et al. (2008) reported a total of 1160 observations from four previous cruises in the BA region, which took place in Aug-Sep 1993 (*NB Palmer*), Dec 1993-Feb 1994 (*Akademik Fedorov*), Sep-Oct 1994 (*NB Palmer*), and Aug-Sep 1995 (*NB Palmer*). These provided data on the sea ice thickness and snow depth distributions (in the period of 1993-1995) for the BA region for the winter (JJA), spring (SON), and summer (DJF) seasons, but not for autumn (MAM). Recently, the March 2003 cruise (*JC Ross*) (Banks et al. 2006), which had Autonomous Underwater Vehicle transects under the limited ice at that time, and the SIMBA 2007 cruise (*NB Palmer*) in Sept-Oct 2007, discussed here, have entered the BA sector for field studies. These last two cruises have also been in the period (2003-present) when the ICESat altimeter was in operation. The timing of the ICESat 2007 missions was selected to be from 2 Oct to 5 Nov,

2007 to overlap when the SIMBA cruise was taking ground measurements. An Australian program (*Aurora Australis*), SIPEX, also coincided with these measurements in the east Antarctic region (Lieser et al., 2010).

Current studies (e.g., Kwok and Cunningham, 2008; Zwally et al., 2008) to derive ice thickness using ICESat laser altimetry have focused on upscaling the ICESat elevation/freeboard to a scale of tens of kilometers due to the lack of high resolution snow depth data available in the polar regions. In this way, however, the high spatial resolution of ICESat elevation/freeboard is degraded. Kurtz et al. (2009) presented their algorithm for downscaling the coarse resolution of snow depth products (AMSR-E and snow climatology) to the ICESat footprint scale, for the first time, to derive ice thickness at the ICESat footprint scale for Arctic sea ice. Their method is a significant improvement, although uncertainty could be introduced during the downscaling process from certain assumptions presented in their paper. The method presented in this paper overcomes the difficulties in independently deriving the snow depth at high resolution, by using empirical equations from field measurements that directly relate snow freeboard to ice thickness. It is, therefore, an alternative and efficient approach for producing ice thickness at the high resolution of the ICESat footprint scale.

The purposes of this study are (1) to present the SIMBA 2007 results, in comparing the ship-based sea ice thickness measurements derived from our downward-looking camera, electromagnetic induction sounding, and ASPeCt visual observations as estimations of the regional snow and ice thickness distribution; (2) to analyze *in situ* measurements of snow depth and ice thickness from drilling profiles at the SIMBA stations and to develop regression models to convert snow freeboard to ice thickness based on those direct *in situ* measurements; and (3) to apply those models to ICESat-derived snow freeboard data for estimating the regional ice thickness in direct comparison to the surface/field measurements. Error propagation from field measurements, to the snow freeboard and ice thickness regression model, plus errors from ICESat elevation to snow freeboard derivation, are modeled and discussed. Comparisons with our field measurements and implications for widespread ICESat applications are then discussed.

2. Data and Methodology

2.1 Ice observation camera, EM sounding, and ASPeCt observations

The overview information about the SIMBA 2007 field work is described in Lewis et al. (this issue). Here we only present the camera, EM sounding, and ASPeCt observations taken from the ship along the inbound and outbound cruise tracks to the drift station (Ice Station Belgica) (Figure 2). The ASPeCt protocol was used to conduct qualitative and quantitative hourly observations simultaneously with the inbound track from 24 - 27 September and outbound track from 24-27 October, 2007. Following the ASPeCt protocol (Worby and Allison, 1999), observations were taken every hour over a circle of 1km radius to initially estimate the overall ice concentration to the nearest tenth. Although sea ice is generally observed throughout the hour, the hourly ASPeCt observation was based upon sea ice conditions 10 minutes before and after the hour. Observations included the ice thickness, floe size, ridged area and average ridge height, snow cover type and snow thickness for each ice type, plus meteorological conditions. A maximum of three ice types (primary, secondary, and tertiary) are recorded using a 0.5 m diameter ball as a reference gauge, mounted on the starboard side of the ship, aft of the bridge. A total of 111 ice observations were recorded following the inbound (52 observations) and outbound (59 observations) tracks. Based on the observations, we used equation 1 (Worby et al. 2008) to calculate the mean ice thickness when ridged ice appears.

$$T_i = \frac{R}{2}(5.4S + T_i^{'}) + (1 - \frac{R}{2})T_i^{'} \quad (1)$$

where T_i is the mean ice thickness, R is the fractional coverage of ridges, S is the mean sail height of ridges, and T_i' is the observed level ice thickness.

Our ice monitoring camera system on SIMBA included two cameras (downward-looking and side-looking) to collect continuous video footage of sea ice conditions during underway ice-breaking operations (Weissling et al., 2009). For sea ice thickness measurements, we used the downward-looking camera (or Cam 1, thereafter), located 5.5 m above the waterline, with a field of view (FOV) of 5.4 m on the ice/snow surface. Cam 1 was positioned on the starboard side of the ship directly above the region of ice monitored by the ASPeCt observers for sea ice thickness estimation. The objective of Cam 1 was to capture a nadir view of broken ice floes turned on their side. These upturned ice floes are the result of the ship's hull breaking the ice and turning them sideways. For floes fully turned to vertical, the measured thickness (through Cam 1 image analysis) is the recorded thickness of the floe. In recognition that many upturned floes will not be fully vertical ($<90^o$), we measured only those that appeared to be upturned in the range of 60^o - 90^o. Due to the viewing angle (nadir camera view) measured floe thickness would vary by the $\sin\theta$ (θ being the upturn angle between the ice floe plane and the sea surface) of the true thickness. It was not possible to measure the upturn angle from the imagery, therefore given an assumed distribution of upturn angles (weighted slightly toward the 60^o - 70^o range), we applied a general correction factor of ($T_{measured}$/0.9), i.e., the correction factor being ~ $\sin 65^o$=0.9
The electromagnetic (EM) instrument deployed on the SIMBA cruise was a Geonics Inc. EM-31, the most commonly used EM sounding device for sea ice thickness assessments (Weissling et al., 2010). The EM-31 measurements of ice thickness (Figure 2) along the inbound track began on 25 September at 13:00 GMT and ended on 27 September at 3:41 GMT; the outbound track began on 25 October at 00:29 GMT and ended at 10:33 GMT on 26 October, 2007. The EM-31 for all underway operations was suspended from the ship's starboard-side A-frame, approximately 8.0 m away from the side of the ship and ~ 3.0 m above the sea level, with a FOV ~6-8 m on the snow/ice surface. The precise distance to the snow/ice surface was measured with an ultrasonic ranger (Campbell Scientific) that was attached to the EM 31 carriage. Underway instrument heights, as assessed by the sonic ranger, ranged from a mean of 3 m for the inbound track and 3.4 m for the outbound track. The EM device generates a primary electric field in a coil on one end of the instrument that subsequently induces a secondary electric field in the conductive layer (sea water) below the surface layer of less conductive snow and ice. The induced electrical field is detected by the coil at the opposite end of the instrument. The strength of the secondary electric field is proportional to the distance from the device to sea water under the ice. The sonic ranger gives the distance to the top surface, which is subtracted from the total distance to the ice-seawater interface, giving the combined snow and ice thickness as an output measurement. More details about the calibration and operation of the EM 31 are described elsewhere (Weissling et al., this issue). Due to known EM sounding underestimation of thick, ridged ice (Pfaffling et al., 2007; Reid et al., 2006), all underway EM thickness estimations were adjusted according to equations (2) and (3). These equations were empirically derived from measured snow and ice thickness data from the co-located and concurrent drilled holes and EM 31 sounding transects at the Fabra site during the 24-day drift period (Weissling et al., this issue).

$$EM_{adjusted} = (EM_{original} + 0.0084)/1.0469, \text{ for } EM_{original} \leq 2.4 \text{ m} \quad (2)$$

$$EM_{adjusted} = (EM_{original} - 1.5)/0.3828, \text{ for } EM_{original} > 2.4 \text{ m} \quad (3)$$

2.2 *In situ* measurements of snow depth, ice freeboard, and ice thickness

During the SIMBA drift station experiment and the underway approach to the drift station, *in situ* measurements of snow depth, ice freeboard, and ice thickness (drilled) were made along profiles of 100 - 300 m at 1-5 m intervals at three inbound ice stations (Station 1, Station 2, and Station 3) and at three drift station sites (Fabra (F), Brussels (B) site, Patria (P) site) (Figure 2). The Brussels and Liege (L) sites were also Ice Mass Balance (IMB) Buoy sites. Liege is only an IMB site without profile measurements, and measurements of ice

thickness at the Patria site were only from EM induction, so these two sites are not included in the analysis. Details about the measurements and techniques are described in Lewis et al. and Weissling et al. (2010). By adding the ice freeboard and snow depth measurements together, snow freeboard values were then derived.

2.3 ICESat Altimetry data for the SIMBA period

NASA's ICESat (Ice, Cloud, and land Elevation Satellite) mission launched in January 2003 has been the only laser altimeter used for mapping and monitoring the Earth's land and ice surface elevations (Zwally et al. 2002; Schutz et al., 2005). The altimeter gives ~2 cm in elevation precision over flat/smooth ice surfaces within 70 m footprints spaced 172 m along track (Zwally *et al., 2008; Kwok et al., 2006)*. During the SIMBA and SIPEX experiments in 2007, NASA adjusted the ICESat Laser 3i campaign schedule (Oct 2-Nov 5, 2007) to fully utilize the field measurements in the West Antarctic (SIMBA) and East Antarctic (SIPEX) for the calibration and validation of ICESat ice thickness algorithms and/or products. Figure 2 shows six cloud-free ICESat tracks from 4-28 October, overlapping the SIMBA field area and the time period. We derived snow freeboard from the ICESat altimetry data using very thin ice or open water leads as a reference for sea level, a so-called along-track filtering method documented in detail in Zwally et al. (2008).

3. Results

3.1 Comparison between camera records, EM 31 and ASPeCt Observations

Datasets from the ASPeCt ice observations, Cam 1, and EM-31 were processed individually to establish ice thickness distributions from each method. The optimal approach for evaluating correlations among different methods is to compare the thickness distributions resulting from them.

A total of 111 ASPeCt observations (52 inbound and 59 outbound) were conducted during the SIMBA cruise. Figure 3 shows that ice thickness generally increases along north-south transects (approximately along the 90° W longitude) and that ice floes with ridges (or ridges counted) are, overall, thicker than level ice only. This is similar to that reported by Worby et al. (2008) along a north-south transect along 165°W in the Ross Sea. SIMBA data showed a thickness transition for the inbound track at 69.2°S and for the outbound track at 68.8°S, where much higher thickness (up to 3-3.5 m) was observed towards the south (ridged first year and multi-year ice) and much thinner ice towards the north (new first year ice). Overall, for the inbound track from the ice edge towards 69.2°S, the mean level ice thicknesses were approximately 10 cm with ~2% ridged ice, only slightly increasing the mean thickness. During this period, the ship traveled primarily through the marginal ice zone, with new ice types of frazil, nilas, brash, and pancake ice. However, in the outbound track from 68.8°S north towards the ice edge, the ice thickness varied from 20 cm to 54 cm, without ridged ice. Broken-up first year ice and pancake ice were the dominant ice types during this period, with some brash and nilas, indicating new ice formation in the region over the ~ 27 days between the inbound and outbound tracks.

Figure 4 shows the frequency distribution of mean ice thickness (ridges counted) and snow depth from all 111 ASPeCt observations. It shows two ice thickness peaks at 0.1 m and 1.7 m, a lower broad peak centered between 2.5 and 2.9m, and one snow depth peak at 0.5 m. The 0.1 m ice thickness peak is attributed to new ice types (frazil, nilas, brash, and pancakes), largely present in the marginal ice zone. The 1.7 m peak shows first year ice with some multi-year ice, while the broad lower peak between 2.5-2.9 m indicates thicker multi-year ice. The overall mean of ice thickness from all observations is 1.54 m, and median is 1.57 m. The mean of the snow depth is 0.41 m, and median is 0.4 m.

The ice thickness distribution from Cam 1 (Figure 5) shows a single-peak, near normal distribution, slightly tailing to the right (mean 0.78 m, median 0.74 m, mode 0.87 m, STD 0.26 m, min 0.14 m, max 2.1m, from 1296 samples), and is much different from the distribution of the ASPeCt observations (Figure 4). Over 93% of the thicknesses from the Cam 1 dataset were between 0.4-1.2 m. This perhaps indicates a bias based on

the ship's ice breaking capability, which is a limitation in using the downward-looking cameras for measuring ice thicker than 1.2 m, although it produces good results for thinner ice floes (Toyota et al., 2004). The major reason for the limitation is that this technique depends on the blocks viewed that are broken at the ship's bow and turned as they are pushed along the ship's side. From Toyota et al. (2004), most research vessels' ice breaking capability to vertically shear sea ice, and thus present full clean edges of upturned blocks, is at approximately 1.0 m. Therefore, sea ice > 1.0 m is likely to shear along gap layers or weak layers (often seen as banding) in the ice. Banding features, common for older thicker multiyear ice, have a propensity to break off or shear along these planes. Therefore, upturned blocks may be representative of only partial thicknesses of the floe. This results in an overall underestimate of the ice thickness distribution, especially when the ship is traveling through perennial ice (> ~1.50m). Underestimation bias may also result from following refrozen leads in pack ice, resulting in overturned blocks being thinner than the nearby ice floes. Furthermore, thin ice types (a few centimeters thick, i.e. nilas) are more likely to be finger-rafted during ice-breaking rather than upturned. These issues may influence the use of downward-looking cameras in capturing both thin and thick ice types, therefore underestimating the frequency of both thin (≤10 cm) and thick (>1.0 m) ice types (Toyota et al., 2004). Our results confirm their findings, that the camera is biased toward sampling this particular range of ice thicknesses.

Figure 6 shows the distribution of EM 31 derived ice and snow thickness for the inbound (907 measurements, left panel) and outbound (1243 measurements, right panel) tracks. Both the original thickness distribution (top panel) and adjusted distribution (bottom panel) for inbound and outbound tracks are near normal distributions, slightly tailing to the right, and are very similar, in terms of shape, mean, and median, but with much larger maximum values from the adjusted EM data (Table 1). The maximum values of 6-7 m (less than 0.01 frequency of occurrence) in the adjusted data are reasonable based on our field experiences in the Antarctic. For example, the EM 31 was raised several times in this cruise to avoid collision with heavily ridged ice even though it was already ~3 m above the level surface. Therefore, the following analyses dealing with EM 31 thickness are based on the adjusted EM 31 data (Figure 6C, D).

Figure 7 shows the ASPeCt distribution of ice and snow thickness for the same two periods when the EM device was in operation. Only 25 and 27 ASPeCt observations were synchronous with the EM dataset during inbound and outbound periods, respectively. Overall, the ASPeCt distributions of thickness are different from the EM dataset, in terms of the shape, mean, median, minimum, and maximum values. The mean, median, and minimum from ASPeCt, are 2.82, 2.9, 1.5 m respectively along the inbound track and 2.37, 2.09, and 1.61 m respectively along the outbound track. These are much larger than those from the EM device, which are 1.53, 1.37, and 0.1 m respectively along the inbound track and 1.46, 1.27, and 0.2 m respectively from the outbound track. The differences however are explainable. Since the ship's path, particularly in the heavy ice in the south (Figure 3), was in general along open leads or thinner ice, the ice being measured by the EM 31, while ASPeCt observations includes a much broader sampling area (radius of 1 km as per ASPeCt protocols). The shape of the distribution from the ASPeCt data is also different from the EM, with a near normal distribution (peak at 3 m), slightly tailing to the left for the inbound track (Figure 7-A) and two peaks (1.8-2 m and 3.4 m) for the outbound track (Figure 7-B). Table 2 summarizes the statistics of the corresponding 45 hours from both EM 31 and ASPeCt data. The greater ice thickness from ASPeCt suggest that the ship was traveling in relatively thick first-year and multiyear ice when the EM 31 was in operation. It is therefore understandable that the ship's track is biased toward thinner ice, which may cause the EM 31 to oversample thinner ice compared to the thicker ice surrounding the narrow track in particular regions.

Since the ASPeCt observations are hourly data (spanning 10 minutes before and after the hour), the EM measurements during the same observation interval were averaged for a more direct comparison with the ASPeCt data. On an average basis, the differences between the EM data and the ASPeCt results were not entirely explainable, since portions of the track were in relatively thinner ice where differences between the EM

and the ASPeCt data could not be explained by "lead bias". We therefore re-examined one portion of the track to compare the EM and ASPeCt observations for these more homogeneous conditions. The ASPeCt observation was also computed in a different manner to provide more detail in this comparison. Each ASPeCt observation was assigned ten thickness values based on the proportional partial concentrations of each ice type. Each ice type was further subdivided into the level and ridged portions, with a ridged thickness computed by Equation 1. This ridged ice thickness was then assigned to the proportion of the area covered by ridges. In a simple example of one ice type in an hourly observation at 100% ice concentration, a single level ice thickness of 1m with a 10% ridged ice area would be assigned nine (virtual) measurements of 1m thickness and one measurement of ridged thickness (Eqn 1). A thickness distribution was then constructed by summing the total number of observations in the period overlapping with the EM measurements. Figure 8 for Oct 25th (18 hourly observations), when homogeneous first year ice floes were the dominant ice type, shows that the two distributions are very similar, in terms of the overall shape and mode (1.2 m for ASPeCt and 1.3 m for EM 31). Differences are observed at either end of the distribution where the EM dataset indicates either thinner (low end) or thicker (high end) ice thickness values as compared with the ASPeCt observations. The EM also continuously measures the thickness variations while the ASPeCt observations are binned into categories on a coarser scale both temporally and spatially. The EM distribution is therefore smoother than the corresponding ASPeCt distribution. Thus, the EM device, mounted on a ship as in this study, may act as an appropriate supplement for ASPeCt observations rather than the primary measuring device and it should provide reasonable total ice and snow distributions in greater detail where the ship track is unbiased.

3.2. Correlation between snow depth, ice freeboard, and ice thickness measurements from the SIMBA profiles

Table 3 shows details of the total 163 *in situ* measurements conducted at the 5 sites associated with the underway stations and the drift station experiment (Figure 2). It is interesting to see that negative freeboard and slush layers (as illustrated in Figure 1) are the dominant phenomenon in Stations 1, 2, and 3. For the Fabra site, however, although the number (19) of negative freeboard sampling sites (drilled) is smaller than the number (36) of positive (or zero) freeboard sampling sites, the mean ice freeboard is negative. From the elevation and snow depth surveys at Fabra (totally 600 sampling sites), however, the percentage of negative freeboard ranges from 51 to 80% (Weissling et al, 2010), so the smaller percentage at the drilled sites is perhaps only related to the smaller sample size. The Brussels site was the only site that had positive mean ice freeboard (0.032 m). This result that the mean ice freeboard is mostly negative, and is close to zero, during the early to middle spring season of a year, is very important for this region. The absolute values are in the range of a few centimeters (0-3 cm), except in the Stations 1 and 2 where the mean ice freeboard values are between -5 to -9 cm. Therefore, in most of the cases, mean snow depth is actually very close to the mean snow freeboard. The significance of this phenomenon for the Antarctic sea ice and for remote sensing of ice thickness is further discussed later.

Figure 9 shows the frequency distribution of snow freeboard, snow depth, and ice thickness from those 163 measurements. The sampling of only five sites and with a "drilling bias" (easier to drill more holes in thinner ice) suggests these distributions are not regionally representative of the general thickness distribution. It is clear that the three are asymmetrical distributions and are significantly tailing to the right (high values). This confirms that the majority of the measurements were actually in the low end of the distributions, but larger values (due to ridged floes) were indeed encountered in those profiles. So the range of thicknesses may have been effectively sampled even though the distribution (i.e., the peak values) may not. The wide range of measurements is the most important factor for developing efficient empirical equations between those three parameters for applying to ICESat freeboard data used later in the paper. Statistics of snow depth and snow freeboard are very similar (Table 4), as mentioned previously for each site/station (Table 3).

Figure 10 shows the scatter plots, regression equations (4-12), and correlation coefficients between the three parameters (snow depth, snow freeboard, and ice thickness) for all measurements (all dots and black line), for measurements with positive (or zero) ice freeboard only (deep red dots and line), and for measurements with negative ice freeboard only (blue dots and line). An important finding for later analyses is that snow depth and snow freeboard indeed have a very good correlation; R^2 of 0.91 for all measurements (Eqn 4); 0.93 for those with negative ice freeboard (Eqn. 6); and 0.97 for those with positive (or zero) ice freeboard (Eqn 5).

Coefficients of determination between ice thickness and snow freeboard (R^2 =0.58 for those with negative ice freeboard data, 0.73 for all data, and 0.81 for those with positive ice freeboard data, equations 7-9) or between ice thickness and snow depth (0.65, 0.70, and 0.78, respectively, equations 10-12) are not as good as those between snow depth and snow freeboard. But all of them are statistically significant (p-value<0.001). Importantly, we found that the correlations between snow freeboard and ice thickness are always better than those between snow depth and ice thickness, and that all correlations from data with positive (or zero) ice freeboard are better than those from all negative ice freeboard or from mixed positive and negative ice freeboard. The significance of these phenomena is further discussed later.

3.3. From field measurements to ICESat altimetry: error propagation and uncertainty

When converting snow freeboard altimetry data to ice thickness without ground truth measurements, we do not know *a priori* whether there is a positive or negative ice freeboard beneath the snow at each ICESat footprint. Therefore we can only use Equation 7 (in Figure 10), $T_i = 2.8808T_{sn} + 0.2201$, that derived from all *in situ* measurements, for ICESat snow freeboard, in deriving ice thickness.

This model (equation 7) however does not take into account the measurement error of snow depth, snow freeboard, and ice thickness. In addition, ICESat freeboard also has error from both the ICESat elevation measurements and the conversion process from elevation to freeboard (Zwally et al. 2008). In this section, we build a new model to accommodate all the errors and uncertainty.

Based on the previous section, there is a linear relationship between snow freeboard and ice thickness, as

$$y = a + bx, \tag{13}$$

where x is the snow freeboard measurement, y the ice thickness measurement, and a and b are estimated constants. Using field data, both x and y are measured and hence both account for measurement errors. A measurement error model, a modification of the above model, can then be defined, as

$$y = a + b(x + \delta) + e, \tag{14}$$

where e is the error in measuring the ice thickness, y, and δ is the error in measuring the snow freeboard, x. We assume that $\delta \sim n(0, \sigma_\delta^2)$ and $e \sim n(0, \sigma_e^2)$. Here σ_δ and σ_e measure the precision of the errors δ and e, respectively. We use a Bayesian method (see Gelman *et al.* 2004) to estimate the precision as well as the coefficients a and b in the regression model. The Bayesian method has become a very popular statistical tool in modeling and data analysis. The main idea is that practitioners can update the information about unknown quantities by using data and prior knowledge about these quantities. Suppose that prior information is elicited and denoted as a distribution $\pi(\theta)$, where θ is the quantity of interest and let $f(x \mid \theta)$ be the data likelihood about θ. The posterior distribution then follows

$$\pi(\theta \mid x) = \frac{f(x \mid \theta)\pi(\theta)}{m(x)}, \tag{15}$$

where $m(x)$ is the distribution of X, noting that $\pi(\theta \mid x)$ contains all the information about θ given observed data and prior probability distribution (or prior). This distribution is used to make any estimation and prediction about θ.

The priors for the parameters $(a, b, \sigma_\delta^2, \sigma_e^2)$ in equation (14) are all noninformative so that the estimations are minimally affected by the priors (Gelman *et al.* 2004). Specifically, we use the prior suggested in Gelman *et al.* 2004 on σ_e^2. The data analysis is carried out by using the software WinBUGs (http://www.mrc-bsu.cam.ac.uk/bugs/).

Since the precision in measuring the snow freeboard from satellite data would not be the same as that from field data, we use a modified model as

$$z = a + b(x_1 + \delta_1) \tag{16}$$

where x_1 is the snow freeboard from ICESat, *z* is the unobserved ice thickness value to be estimated, and δ_1 is the measurement error of the ICESat freeboard. The reason that we do not add another random error for *z* in (16) is because we do not have any data to support estimation for this precision. Hence we will only use the predicted model (13) and incorporate the extra information about the errors in measuring snow freeboard via ICESat. Such extra information is built up in a prior distribution, $\pi(\sigma_{\delta_1}^2)$, that follows an inverse gamma distribution in which we specify that σ_{δ_1} has a mean of 5 cm and a standard deviation of 1.5 cm. Those numbers are based on the results from Kwok and Cunningham (2008) for the Arctic sea ice, where a mean error of 5 cm in the ICESat freeboard was found. Hence in our research, we use 5 ± 1.5 cm as a reasonable error of ICESat freeboard for our modeling.

In computing the estimations, the Markov chain Monte Carlo (MCMC) method is used (Gelman *et al.* 2004) and the resulting estimations of the coefficient and error parameters are shown in Table 5. By comparing the estimated parameters *a* and *b* with constants from equation 7 (in Figure 10), we found that they are very similar and that both models have the same R^2 of 0.73. The advantage of using the Bayesian method, however, is that for those unknown parameters, including the standard deviation components of the measurement error, σ_δ, and observational error, σ_e, point estimations, standard deviations, as well as the 95% credible intervals can all be obtained (Table 5). For example, the mean measurement error from the field work was 0.0051m (0.51 cm) based on all measurements and our modeling, actually very small; the mean estimated ice thickness error for σ_e in equation (14) is 0.4884 m, which will be propagated into the final ICESat estimated ice thickness error. Although we cannot directly estimate the standard error for *z* since there are no actual thickness measurements in an ICESat footprint, it is believed that error will be larger than 0.49 m for all six tracks used in the study.

3. 4. ICESat snow freeboard and ice thickness and comparisons with other methods

Figure 11 shows the ICESat snow freeboard and ice thickness profile for the track 0011 (Track #2 in Fig.2) (Oct 8, 2007) and frequency distributions of snow freeboard and ice thickness for the track 0011 and for all six tracks together (see figure 2). Table 6 shows their statistics. Overall, there were 1625 and 5115 footprints for the track 0011 and for all tracks, respectively. The percentage of negative freeboard from either the track 0011 or from all tracks is ~0.7%, slightly less than the 1%, based on the algorithm used to calculate snow freeboard from ICESat elevation (Zwally et al. 2008).

From the ICESat track 0011 profile (top panel of figure 11), the freeboard values in the footprint scale 70 m (black color) show big spatial variations. The values can jump, in many cases, from 0 (at the lead) to 20 or 30 cm (on the ice floe) immediately. This is really the advantage of high spatial resolution of ICESat data. If the footprint values are averaged or upscaled to a coarser resolution, the advantage of those details on ice conditions/freeboard variations is lost. For example, although the best resolution of ice thickness distribution is clearly with full resolution (70m), the 1 km running mean profile (red) is still relatively good to catch most of the leads and spatial variations in different ice situations. However, the 12.5 km (pixel size of the AMSR-E snow depth products) running mean profile (blue) averaged all the spatial variations out and is almost a flat line

along the mean of 0.39 m. The 1 km running mean of ice thickness profile (gray) shows well the spatial variations of ice type that change along the track. Several big leads are still clearly shown, such as at 69.62°, 70.15° and 70.23°S. The big thickness jump south of 69.9°S on 8 Oct was evident during the field observations as well as from the ship observations (Figure 3) taken in the first week in October. So in general, the ICESat data are reasonably good and match well with our field experience/observations, even with 1km averaging. The statistics below however, are all based on the footprint scale.

Both snow freeboard and ice thickness from either the track 0011 or from all tracks show very similar and asymmetrical distribution, tailing to higher freeboard and ice thickness, due to highly ridged first year and multiyear ice. Although track 0011, and all other tracks, have a similar median (0.36-0.37 m for snow freeboard and 1.21-1.24 m for ice thickness) and mode (0.34m for snow freeboard and 1.16m for ice thickness), the mode (peak) of freeboard and thickness along track 0011 accounts for 30% and 23% of all measurements, respectively. This is larger than the corresponding 20% and 15% of those from all tracks. These other, mostly shorter, tracks might have passed through some thicker multi-year and ridged first year ice floes, with a much wider range of snow freeboard and ice thickness compared with those along the longer track 0011. The maximum freeboard and thickness from all tracks is 1.94 m and 5.72 m respectively, larger than 1.44 m and 4.30 m from track 0011. The mean freeboard and thickness from all tracks are also slightly larger than those from the track 0011 alone: 0.42 vs 0.39 m for freeboard and 1.38 vs 1.30 m for thickness. We also suggest that a single track alone may insufficiently sample a region such as the Bellingshausen Sea with spatial heterogeneity in ice thickness for an ensemble ice thickness distribution (the N-S gradient in Figs 3 and 11). Conversely even a single track can delineate the boundaries between these regions, in this case between the first year and multiyear ice regions of the Bellingshausen Sea.

Based on the overall separation and distribution of first year ice and multi-year ice from RADARSAT/Envisat images (Figure 5 of Ozsoy-Cicek et al., this issue), plus visual inspection of the freeboard and ice thickness jumps from low values to high values (as seen in Figure 11) along profiles (also in Figure 3 from ship observations), we redo the frequency distributions and statistics for first year ice and multi-year ice separately as shown in Figure 12 and Table 7. Although there is a time separation between the radar images of the 12 Oct and the ICESat tracks spanning 4-28 Oct, we still see quite good separation of the two types. Sharp/high modes of snow freeboard and ice thickness for first year ice (0.34 m and 1.2 m respectively) clearly differ from the relatively flat/wide modes of snow freeboard and ice thickness for the multi-year ice (0.4 m and 1.37 m respectively). Other statistical parameters (mean, median, and maximum values) are also well separated for first year and multi-year ice (Table 7). Multi-year ice has much longer tails to the right indicating the thickest ice mapped by ICESat. The significance of this piece of work is that we might be able to map the first year and multi-year ice by directly using the ICESat freeboard and/or ice thickness data. Further examination of this capability should use radar images (ENVISat) and ICESat tracks within a time difference of 6 hours or less, not what we did here using the Oct 12 radar image for all ICESat tracks from 4 – 28 Oct.

Inter-comparison between ICESat measurements (Figures 11 and 12) and the *in situ* measurements (Figure 9 and Table 4) shows that both the snow freeboard and ice thickness frequency distributions from all field sites and from all ICESat tracks are very similar in shape, with asymmetric distributions and long tails to higher values. A significant difference however is that all statistical parameters for the ICESat data are much larger than those from the field sites, especially the median, mode, and maximum values. This matches well with what we saw in the field, since the few selected profiles were biased toward relatively thinner ice areas given that is where most of the drilled measurements were made.

Inter-comparison between ICESat measurements (Figures 11 and 12) and ASPeCt observations (Figures 3 and 4) shows large differences. While the first peak at 0.1 m from the ASPeCt (Figure 4) was mostly contributed from the marginal ice zone that was not included in the six ICESat tracks (see figure 2), the second peak at 1.7 m of the ASPeCt observations is still larger than the 1.16 m from all ICESat tracks. The mean and

median ice thickness from all ASPeCt observations are respectively 1.54 and 1.57 m, and are slightly larger than the 1.38 and 1.24 m from the ICESat. Considering that the ASPeCt observations are hourly data and could miss many variations of ice situations between the hours, is supported by the fact that the ice thickness range from 0.4-1.2 m accounts for less than 10% of all ASPeCt observations (figure 4). A factor in the thick ice zones such as the location of the Ice Station Belgica floe is the possible overestimation of ice thickness from the ASPeCt observations. Using the floe as an example, when we arrived at the floe, the last ASPeCt observation characterized it as a single ice type, multiyear ice with thickness (level ice) of 2m. From the drilling profiles however, we found that there were actually three zones of ice thickness embedded in the single floe, with means of 0.6m, 1.1m and 2.3m (Lewis et al., this issue). An area-weighted mean thickness gave the overall mean thickness of the entire floe to ~1.39m, i.e. substantially less than the >2m estimated from the ASPeCt observation. These multiyear and thick first year floes are typically composites of thin and thick ice at sub km scales. We hypothesize that these thickness variations are apparently are not resolved sufficiently by the ASPeCt visual typing which assigns a single ice type and thickness at the ~1km scales of the floe boundaries. Since the IEESat samples at 170m intervals, it would sample instead about five different sites within this 1km scale, hypothetically leading to better resolution of the thin ice components within that scale and consequently lowering the mean thickness at that scale. From Figure 11 (top), the region of multiyear ice estimated from ICESat at latitudes greater than 70 degrees, had many values of thinner ice thicknesses that were also typically found north of the thick ice regime. When averaged together, these values overall lower the mean thickness. The maximum ice thickness of 3.5 m from the ASPeCt, however, is less than 5.80 m from the ICESat. This is expected, since ICESat tracks could pass over the large multiyear ice zone while the vessel was on its outer boundary. However, the mean and median snow depth from ASPeCt are 0.41 m and 0.4 m respectively, which are very similar to the mean and median snow freeboard 0.42 m and 0.37 m from all ICESat data (Table 6).

Compared with the EM 31 measurements of combined snow and ice thickness from the inbound and outbound tracks (figure 6-C, D and table 1), ICESat measurements (ice thickness and snow thickness/freeboard) from all tracks (Table 6) are larger than EM 31 measurements, i.e., 1.80 m vs 1.46 m for mean, 1.61 m vs 1.36 m for median, and 1.50 m vs 1.33 for mode. But if we only compare ICESat first year ice (Table 7) with EM 31 data, 1.35 m vs 1.46 m for mean, 1.31 vs 1.36 for median, 1.54 vs 1.33 m for mode, we find they are actually very similar. This suggests that EM 31 may predominantly represent the first year ice, although it might have encountered a few multi-year ice floes and/or highly ridged first year ice to make the maximum ice thickness up to 7.36 m. This is much larger than the maximum value of 4.04 m from the ICESat first year ice, but only slightly less than the 7.74 m maximum value from the ICESat multi-year ice (Table 7).

As mentioned in the introduction, of the 1160 ASPeCt observations from four previous cruises in the BA region, 485 were in the spring season (September, October, November) (Worby et al. 2008). The asymmetrical unimodal distribution of ice thickness derived from these 485 observations, tailing to the right (Figure 4 of Worby et al. 2008), is actually very similar to the ICESat distribution presented here, but with a much lower mean and maximum than all ICESat data (Table 6), respectively 0.79 m vs 1.38 m for mean ice thickness, and 3.6 m vs 5.8 m for maximum ice thickness. The mean snow depth on sea ice was 0.17 m, which is less than the 0.42 m mean snow freeboard from ICESat. The difference between the ASPeCt observations (1993-1995) and ICESat (2007), as well as ASPeCt (2007), is mainly due to that the ASPeCt observations in 1993-1995 came from a much larger area and were mostly from first year ice. If we compared them with the ICESat first year ice (Table 7), the numbers are much closer, i.e., 0.79 vs 1.06 m for mean ice thickness, 3.6 vs 2.98 m for maximum ice thickness, 0.17 vs 0.29 m for snow depth/freeboard.

4. Summary and Discussion

This paper reports our results from four different surface methods (ASPeCt ship observations, downward looking camera, EM 31, and *in situ* drilling measurements) for snow and ice thickness estimation/measurement

during the SIMBA 2007 experiment. The *in situ* measurements were used to derive a model for estimating ice thickness from snow freeboard, and the model was then applied to ICESat freeboard data to derive ice thickness for the period when ICESat overlapped the SIMBA area. Errors from the *in situ* measurements and from the ICESat freeboard estimation were incorporated into the model, so that a thorough evaluation of the model and uncertainty of the ice thickness estimation from ICESat is possible. Although we cannot estimate the final error propagated into the ICESat ice thickness estimation due to a lack of data in the ICESat footprints, it is believed that the mean error will be larger than 0.49 m from all six tracks used in the study.

Overall, among the three underway observation/measurement methods, the ASPeCt observations are still proven to be the best in providing an overall picture of snow and ice thickness, although, by comparison to the ICESat distribution, ASPeCt might have under-sampled the ice thickness range from 0.4-1.2 m. The EM 31, however, shows reasonable results for homogeneous first year ice, though overall it over-sampled the thinner ice along the ship's track, to avoid thicker ice for reasons related to both safety and cost. Therefore, the EM device can acts as an appropriate supplement for ASPeCt observations rather than the primary measuring device and it can provide reasonable total ice and snow distributions under fairly homogeneous ice conditions. The downward looking camera in general is limited to ice less than 1 m thickness which is equal to the ship's capability to vertically shear sea ice.

The snow freeboard and ice thickness distributions derived from ICESat for the study area seem reasonable as presented in section 3.4; in addition, it is possible to separate first year from multi-year ice based on the freeboard and/or ice thickness, with information from near concurrent radar images. This is very encouraging for us to further explore the possibility in deriving different empirical equations of snow freeboard and ice thickness for different Antarctic sectors and in different seasons, from all available profile data collected in the Antarctic region. Therefore, better ice thickness data at the ICESat footprint scale will be able to be produced in the near future.

In situ measurements from drilled transects are the best way to provide precise thickness and other physical properties of snow and ice, but it is difficult work and at a very local scale. From profiles at the five SIMBA stations we found that, in general, during early to middle spring, the mean ice freeboard is mostly negative and is close to zero, which suggests that the mean snow depth is actually very close to the mean snow freeboard. This has significant implications for estimating the thickness of Antarctic sea ice from radar and laser altimetry using the buoyancy equations, since the most difficult task for estimating ice thickness from altimetry is determining the snow depth (Kurtz et al. 2009). Using either the AMSR-E snow depth or snow climatology would bring considerable uncertainty (error) to the estimation of ice thickness. From these field measurements and many others (e.g. Jeffries et al, 2001; Perovich et al, 2004; Hass et al., 2001; Maksym and Jeffries, 2000, 2001; Lange et al., 1990; Eicken et al., 1995), we understand that the situation where the ice freeboard is very close to zero, and that snow freeboard approximately equals snow depth may be generally applicable in the Antarctic. Therefore, we postulate the use of snow freeboard derived from ICESat as snow depth and apply those isostatic equations to derive the ice thickness as a physical model for computing Antarctic ice thickness from altimetry.

The near perfect linear correlation between snow depth and snow freeboard found in this paper (Figure 10-A) differs significantly from the Arctic case presented in Kurtz et al. (2009). In our case, the linear relationship goes up to 1.5 m in snow depth and 1.2 m in snow freeboard. In their Arctic experiment at the 12.5 km scale using freeboard values from Airborne Topographic Mapper (ATM) and snow depth values from Polarimetric Scanning Radiometer (PSR) mounted on the same NASA P-3 aircraft, they found that there is a cutoff freeboard value, ~25 cm, where snow depth stops increasing as snow freeboard increases. This indicates the significant difference of the snow depth and snow depth/freeboard relations between the Arctic and Antarctic, since the snow depth in the Arctic is usually much lower (Connor et al. 2009 and Kurtz et al., 2009). In the Antarctic sea ice, the snow depth can be easily up to 1 m to 1.5 m as indicated at our SIMBA sites and the

snow freeboard and snow depth are linearly correlated and are very similar. This further suggests the merit of our idea mentioned above, to replace snow depth using ICESat snow freeboard (or using the derived snow depth and freeboard equations 4-6 in figure 10-A) in those isostatic equations to derive ice thickness for Antarctic sea ice.

The multiplying constant in Equation 5 (and in Figure 10) is 1.0114 (i.e., close to 1), which means that we can almost estimate the snow freeboard using snow depth plus 0.0362 m for cases when the ice freeboard is positive or zero (model 1 of Figure 1). For those negative ice freeboard cases (model 2 of Figure 1), the snow freeboard is actually about 0.8033 times the snow depth, plus 0.004 m (Eqn 6 in Figure 10). For those negative ice freeboards with slush layers (model 3 of Figure 1), the snow freeboard is the snow depth. In this paper, we actually did not separate the last two cases (models 2 and 3) and have treated them as one case. For future work, we should separate them to derive different empirical equations.

As we found, all correlations from data with positive (or zero) ice freeboard are better than those from data with negative ice freeboard, or from data of mixed positive and negative ice freeboard (Figure 10). This has significant implications for ice thickness derivations from airborne or satellite-borne altimetry data such as the ICESat and Cryosat-2, particularly for Antarctic sea ice where negative ice freeboards are very common (Lytle and Ackley 1996; Golden et al 1998; Maksym and Jeffries, 2000, 2001; Lange et al., 1990). If negative ice freeboard (and/or slush layer) can be mapped spatially and temporally from space, different equations could and should be separately applied to different cases. This will be addressed in our future work.

As mentioned in the introduction, current studies to derive ice thickness using ICESat laser altimetry have focused on upscaling the ICESat elevation/freeboard data to scales of tens of kilometers due to the lack of high resolution snow depth data in the polar regions. The algorithm by Kurtz et al. (2009) downscales the coarse resolution of snow depth products (AMSR-E or snow climatology) to ICESat footprint scales using a cutoff freeboard and iteration approach to meet the mean snow depth constraints of AMSR-E or snow climatology. While this might work well in the Arctic sea ice, it is not appropriate for the Antarctic sea ice, for three reasons: (1) there is not a cutoff snow freeboard in Antarctic sea ice as there is in the Arctic sea ice; (2) the snow climatology for Antarctic sea ice is on the scale of hundreds of kilometers with no measure of interannual variability (Worby et al 2008), and it is orders of magnitude coarser than AMSR-E and does not have the small-scale variability crucial for prediction of high-resolution ice thickness; and (3) AMSR-E snow depth products are not well validated, have low resolution (12.5km) and have a limitation on snow depth over 50 centimeters.

Therefore, our approaches: (1) of using empirical equations based on *in situ* measurements in relating snow freeboard to ice thickness and (2) of using isostatic equations that replace snow depth with snow freeboard (or empirical equations that convert freeboard to snow depth), should be efficient and important ways to derive ice thickness for Antarctic sea ice from ICESat/Cryosat-2 in their footprint scales. We believe this is a significant contribution from this paper to this community.

Acknowledgment

This research was supported by a U.S. NSF Grant (#AWT0703682), a NASA Grant (#NNX08AQ87G) and a grant from the College of Business at UTSA. We gratefully acknowledge the team of ice observers on the SIMBA cruise and the NASA's effort and coordination in adjusting the ICESat Laser 3i campaign schedule to fully utilize the field measurements. We are very grateful to the three anonymous reviewers and editor Tony Worby for their helpful comments and suggestions to improve the paper.

References

Banks, C., Brandon, M.A., Garthwaite, P.H., 2006. Measurement of sea-ice draft using upward looking ADCP on an Autonomous Underwater Vehicle. Annals of Glaciology 44(1), 211-216.

Comiso, J., Nishio, F., 2008. Trends in the sea ice cover using enhanced and compatible AMSR-E SSM/I and SMMR Data. Journal of Geophysical Research 113, C02S07, doi:10.1029/2007JC004257.

Comiso, J., Cavalieri, D.J., Markus,T., 2003. Sea ice concentration, ice temperature, and snow depth using AMSR-E data. IEEE Transactions on Geoscience and Remote Sensing 41 (2), 243-252.

Conner, L.N., Laxon, S.W., Ridout, A.L., Krabill, W.B., McAdoo, D.C., 2009. Comparison of EnviSAT radar and airborne laser altimeter measurements over Arctic sea ice. Remote Sensing of Environment 113, 563-570.

Eicken, H., Fischer, H., Lemke, P., 1995. Effects of the Snow Cover on Antarctic Sea Ice and Potential Modulation of its Response to Climate Change. Annals of Glaciology 21, 369-376.

Gelman, A., Carlin, J.B., Stern, H.S., Rubin, D.B., 2004. Bayesian data analysis. Chapman and Hall/CRC, New York, USA.

Giles, K. A., Laxon, S.W., Wingham, D. J., Wallis, D.W., Krabill,W. B., Leuschen, C. J., McAdoo, D., Manizade, S.S., and Raney, R.K, 2007. Combined airborne laser and radar altimeter measurements over the Fram Strait in May 2002. Remote Sensing of Environment 111 (2-3), 182-194.

Giles, K. A., Laxon,S.W., Ridout, A.L., 2008. Circumpolar thinning of Arctic sea ice following the 2007 record ice extent minimum. Geophysical Research Letters 35, L22502, doi:10.1029/2008GL035710.

Giles, K.A., Laxon, S.W., Worby, A.P., 2008. Antarctic sea ice elevation from satellite radar altimetry. Geophysical Research Letters 35 (3), doi:10.1029/2007GL031572.

Golden,K.M, Ackley, S.F., Lytle,V.I., 1998. The percolation phase transition in sea ice. Science 282 (5397), 2238 - 2241.

Haas, C., Thomas, D.N., Bareiss, J., 2001. Surface properties and processes of perennial Antarctic sea ice in summer. Journal of Glaciology 47, 613-25.

IPCC-C4, 2007, Lemke, P., Ren, J. Alley, R.B., Allison, I., Carrasco, J., Flato, G., Fujii, Y., Kaser, G., Mote, P., Thomas, R.H., Zhang, T., 2007. Observations: Changes in Snow, Ice and Frozen Ground. In: Climate Change 2007: The Physical Science Basis. Contribution of Working Group I to the Fourth Assessment Report of the Intergovernmental Panel on Climate Change. [Solomon, S., D. Qin, M. Manning, Z. Chen, M. Marquis, K.B. Averyt, M. Tignor and H.L. Miller (eds.)]. Cambridge University Press, Cambridge, United Kingdom and New York, NY, USA.

Jeffries, M.O., Kroise, H.R., Hurst-Cushing, B., Maksym, T., 2001. Snow ice accretion and snow cover depletion on Antarctic first-year sea ice floes. Annals of Glaciology 33, 51-60.

Kwok, R.; Zwally, H. J., Yi, D., 2004. ICESat Observations of Arctic Sea Ice: A First Look. Geophysical Research Letters 31, L16401, doi:10.1029/2004GL020309.

Kwok, R., Cunningham, G.F., Zwally, H.J, and Yi, D., 2006. Ice, Cloud, and land Elevation Satellite (ICESat) over Arctic sea ice: Retrieval of freeboard. Journal of Geophysical Research 112, C12013, doi:10.1029/2006JC003978.

Kwok, R., 2007. Near Zero Replenishment of the Arctic multiyear sea ice cover at the end of 2005 summer. Geophysical Research Letters 34, L05501, doi:10.1029/2006GL028737.

Kwok, R., Cunningham, G.F., 2008. ICESat over Arctic sea ice: Estimates of snow depth and ice thickness. Journal of Geophysical Research 113, C08010, doi:10.1029/2008JC004753.

Kurtz, N. T., Markus, T., Cavalieri, D.J., Sparling, L.C., Krabill, W.B, Gasiewski, A.J., Sonntag, J.G., 2009. Estimation of sea ice thickness distributions through the combination of snow depth and satellite laser altimetry data. Journal of Geophysical Research 114, C10007, doi:10.1029/2009JC005292.

Lange, M.A., Schlosser, P., Ackley, S.F. Wadhams, P., Dieckmann, G., 1990. $\delta^{18}O$ concentrations in sea ice of the Weddell Sea. Journals of Glaciology 36, 315-323.

Lewis, M. J., Tison, J. L., Weissling, B., Delille, B., Ackley, S. F., Brabant, F., Xie, H., 2010. Sea ice and snow cover characteristics during the winter-spring transition in the Bellingshausen Sea: an overview of SIMBA 2007. Deep Sea Research, this issue.

Lytle, V., Ackley, S.F., 1996. Heat flux through sea ice in the western Weddell Sea: convective and conductive transfer processes. Journal of Geophysical Research 101 (C4), 8853-8868.

Markus, T., Cavalieri, D.J., 1998. Snow depth distribution over sea ice in the Southern Ocean from satellite passive microwave data, in Antarctic sea ice: physical processes, interactions and variability. American Geophysical Union, Antarctic Research Series 74, Washington, D. C., USA, 19-39.

Maksym, T., Jeffries, M.O., 2000. A one-dimensional percolation model of flooding and snow-ice formation on Antarctic sea ice. Journal of Geophysical Research 105 (C11), 26313-26332.

Maksym, T., Jeffries, M.O., 2001. Phase and compositional evolution of the flooded layer during snow-ice formation on Antarctic sea ice. Annals of Glaciology 33, 37-44.

Ozsoy-Cicek, B., Kern, S., Ackley, S.F., Xie, H., Tekeli, A.E., 2010. Intercomparisons of Antarctic sea ice properties from ship observations, active and passive microwave satellite observations in the Bellingshausen Sea. Deep Sea Research, this issue.

Pfaffling, A., Haas, C., Reid, J. E., 2007. A direct helicopter EM sea ice thickness inversion, assessed with synthetic and field data. Geophysics 72, doi:10.1190/1.2732551.

Perovich, D.K., Elder, B.C., Claffey, K.J., Stammerjohn, S., Smith, R., Ackley, S.F., Krouse, H.R., Gow, A.J., 2004. Winter sea-ice properties in Marguerite Bay, Antarctica. Deep Sea Research, Part II (51), 2023-2039.

Powell, D.C., Markus, T., Cavalieri, D.J., Gasiewski, A.J., Klein, M., Maslanik, J.A., Stroeve, J.C., Sturm, M., 2006. Microwave signature of snow on sea ice: modeling. IEEE Transactions on Geoscience and Remote Sensing 44 (11), 3091-3102.

Reid, J. E., Pfaffling, A., Worby, A.P., Bishop, J.R., 2006. In situ measurements of the direct-current conductivity of Antarctic sea ice: implications for airborne electromagnetic sounding of sea-ice thickness. Annals of Glaciology 44, 217-223.

Rothrock, D. A., Yu, Y., Maykut, G. A., 1999. Thinning of the Arctic sea ice cover. Geophysical Research Letters 26 (23), 3469–3472.
Rothrock, D.A., Zhang, J., Yu,Y., 2003. The arctic ice thickness anomaly of the 1990s: A consistent view from observations and models. Journal of Geophysical Research 108 (C3), 3083, doi:10.1029/2001JC001208.
Schutz, B. E., Zwally, H.J., Shuman, C.A., Hancock, D, DiMarzio, J.P., 2005. Overview of the ICESat Mission. Geophysical Research Letters 32, L21S01, doi:10.1029/2005GL024009.
Stroeve, J., Holland, M., Meier,W., Scambos,T., Serreze, M., 2007. Arctic sea ice decline: Faster than forecast. Geophysical Research Letters 34, L09501, doi:10.1029/2007GL029703.
Stroeve, J., Frei, A., McCreight, J., Ghatak, D., 2008. Arctic sea-ice variability revisited. Annals of Glaciology 48 (1), 71-81.
Tucker, W.B., Weatherly, J.W., Eppler, D.T., Farmer, L.D., Bentley, D.L., 2001. Evidence for rapid thinning of sea ice in the western Arctic Ocean at the end of the 1980's. Geophysical Research Letters 28 (14), 2581-2854.

Wadhams, P., Davis, N. R., 2000. Further evidence of ice thinning in the Arctic Ocean, Geophysical Research Letters 27 (24), 3973– 3975.

Weissling, B., Ackley, S., Wagner, P., Xie, H., 2009. EISCAM – Digital image acquisition and processing for sea ice parameters from ships. Cold Regions Science and Technology 57 (1), 49-60.

Weissling, B., Lewis, M.J., Ackley, S.F., 2010. Sea ice thickness and mass at Ice Station Belgica, Bellingshausen Sea, Antarctica. Deep Sea Research, this issue.

Worby, A. P., Allison, I, 1999. A technique for making ship-based observations of Antarctic sea ice thickness and characteristics, Part I: Observational technique and results. Antarctic CRC Research Report 14, 1-23.
Worby, A. P., Geiger, C., Paget, M., Van Woert, M., Ackley, S., DeLiberty, T., 2008. Thickness distribution of Antarctic Sea Ice. Journal of Geophysical Research 113, C05S92, doi:10.1029/2007JC004254.

Zwally, H.J., Schutz, B., Abdalati, W., Abshire, J., Bentley, C., Brenner, A., Bufton, J., Dezio, J., Hancock, D., Harding, D., Herring, T., Minster, B., Quinn, K, Palm, S., Spinhirne, J., Thomas, R., 2002. ICESat's laser measurements of polar ice, atmosphere, ocean, and land. Journal of Geodynamics 34 (3-4), 405-445.

Zwally, H. J., Yi, D., Kwok, R., Zhao, Y., 2008. ICESat measurements of sea ice freeboard and estimates of sea ice thickness in the Weddell Sea. Journal of Geophysical Research 113, C02S15, doi:10.1029/2007JC004284.

Table 1. Statistics of the EMI 31 snow and ice thickness (m) for both original and adjusted for the inbound and outbound tracks

Statistics	Inbound (907 samples)		Outbound (1243 samples)	
	Original	Adjusted	Original	Adjusted
Mean (95% confidence interval)	1.50 (1.46-1.55)	1.53 (1.47-1.58)	1.44 (1.40-1.48)	1.46 (1.41-1.51)
Standard deviation	0.02	0.03	0.02	0.03
Median	1.43	1.37	1.32	1.27
Mode	1.35	1.33	1.32	1.15
Max	3.90	6.26	4.32	7.36

Table 2. Statistics of the EMI 31 and ASPeCt snow and ice thickness (m) in corresponding hours (45 hours) for the inbound and outbound tracks

Statistics	EMI 31	ASPeCt
Mean (95% confidence interval)	1.44 (1.31-1.57)	2.56 (2.46-2.76)
Standard deviation	0.43	0.67
Median	1.39	2.77
Mode	1.51	1.9 and 3.4
Max	3.11	3.73

Table 3. Details of field-based profile measurements from the SIMBA 2007 experiment

	Number of measurements	Number of Negative ice freeboard	Mean ice freeboard (m)	Mean Snow depth (m)	Mean Snow freeboard (m)	Mean Ice thickness (m)
Station 1	21	19	-0.089	0.411	0.322	1.008
Station 2	16	12	-0.059	0.528	0.472	1.707
Station 3	7	7	-0.025	0.240	0.215	0.629
Fabra site	55	19	-0.023	0.651	0.628	2.104
Brussels site	64	1	0.032	0.097	0.129	0.561
Total/mean	163	58	-0.015	0.375	0.361	1.259

Table 4. Statistics of the snow depth, snow freeboard, and ice thickness from the 163 in situ measurements (m) during the SIMBA 2007.

	Snow depth	Snow freeboard	Ice thickness
Mean (95% confidence interval)	0.38 (0.33-0.42)	0.36 (0.32-0.40)	1.26 (1.11-1.40)
Standard deviation	0.32	0.28	0.94
median	0.28	0.26	0.86
mode	0.10	0.20	0.56
min	0.03	0.08	0.47
max	1.48	1.11	4.2

Table 5, the model parameters ($a, b, \sigma_\delta, \sigma_e$) for equations 14 and 16 (unit is meter)

Parameters	Estimation	Standard Deviation	95% Bayesian Credible Interval
a	0.2184	0.0627	(0.0947, 0.3417)
b	2.881	0.1404	(2.616, 3.171)
σ_e	0.4884	0.0267	(0.4396, 0.5432)
σ_δ	0.0051	0.0045	(0.0016, 0.017)

Table 6. Statistics of the ICESat snow freeboard and ice thickness (m) from the 0011 track and from all tracks during the SIMBA 2007, with 0.68% and 0.70% negative freeboard for the 0011 track and for all tracks, respectively.

	Track 0011 (1625 footprints)		All tracks (5048 footprints)	
	Snow freeboard	Ice thickness	Snow freeboard	Ice thickness
Mean (95% confidence level)	0.39 (0.38-0.40)	1.30 (1.28-1.33)	0.42 (0.41-0.42)	1.38 (1.34-1.40)
Standard deviation	0.19	0.54	0.24	0.70
median	0.36	1.21	0.37	1.24
mode	0.34	1.16	0.34	1.16
max	1.44	4.30	1.94	5.80

Table 7. Statistics of the ICESat snow freeboard and ice thickness (m) for the first-year and multi-year ice from the six tracks.

	First-year (1682 footprints)		Multi-year (3366 footprints)	
	Snow freeboard	Ice thickness	Snow freeboard	Ice thickness
Mean (95% confidence level)	0.29 (0.28-0.30)	1.06 (1.04-1.08)	0.48 (0.47-0.49)	1.59 (1.57-1.62)
Standard deviation	0.14	0.40	0.26	0.75
median	0.28	1.03	0.44	1.48
mode	0.34	1.20	0.40	1.37
max	0.96	2.98	1.94	5.80

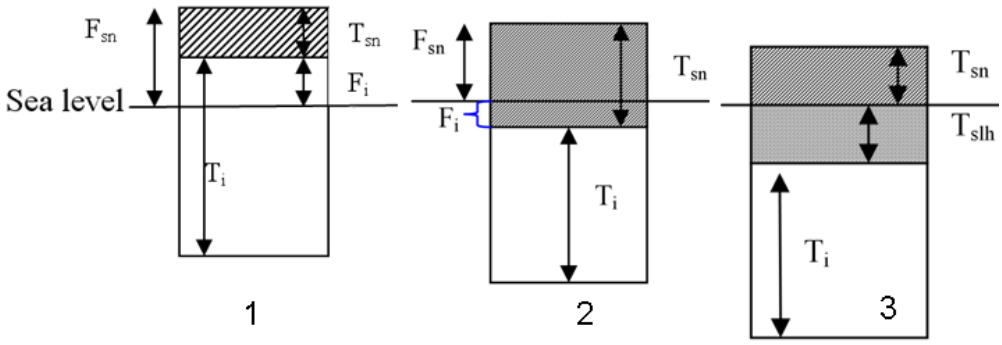

Figure 1. Complex Antarctic sea ice generalized in three models. Model 1 denotes positive snow and ice freeboard and is the common case for the Arctic and found frequently also for Antarctic sea ice. Models 2 and 3 are the dominant cases and unique for Antarctic sea ice (and are rarely found in the Arctic). Model 2 indicates snow-ice surface below sea water level, negative ice freeboard. This situation can last for months in some areas in Antarctic, such as the colder western Weddell Sea (Lytle and Ackley 1996) while for only 2 or 3 days for other areas such as the warmer, thin ice areas of the eastern Weddell Sea (Golden et al 1998). Model 3 is snow/ice interface flooding (or slush layer) which can last for days or months and is very common for all regions and all seasons in Antarctic sea ice. Once frozen (snow to ice conversion), isostatic adjustment will push the new snow-ice interface above sea level, a positive ice freeboard again (as for Model 1). F_{sn} is snow freeboard that can be derived from ICESat laser altimetry, F_i is ice freeboard that can be derived from radar altimetry; T_{sn} is the snow thickness, T_i is the ice thickness, and T_{slh} is the slush layer thickness. In the model 3, T_{sn} equals to F_{sn}.

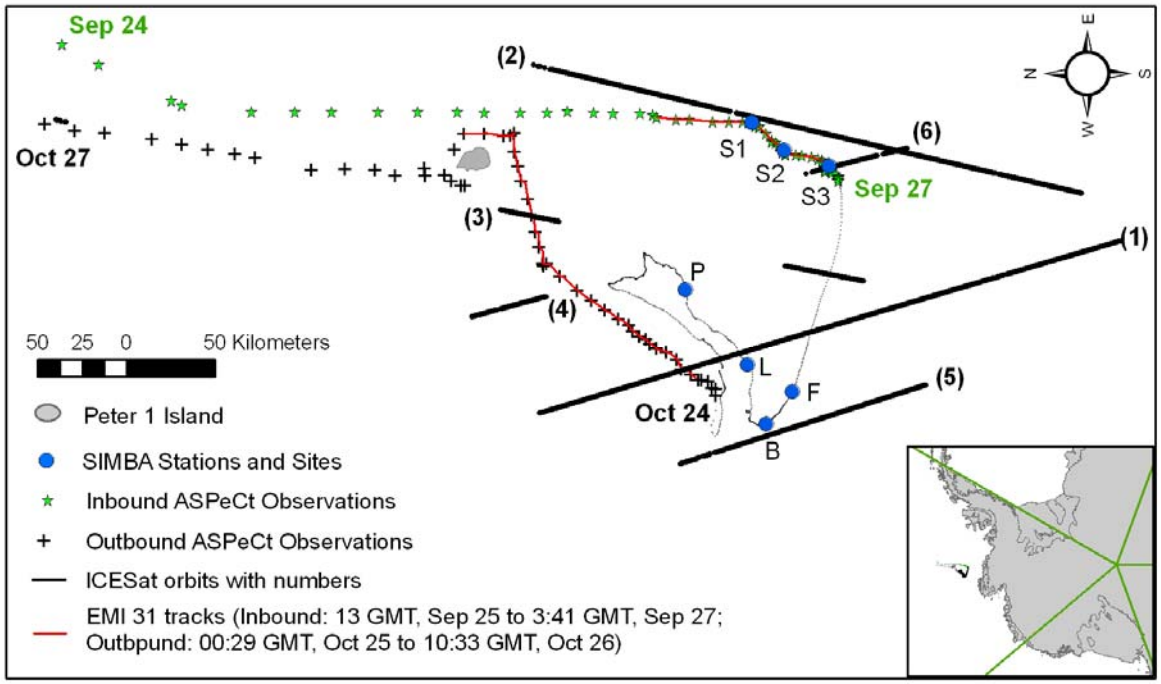

Figure 2. ASPeCt observations, EMI 31 and ICESat tracks of the SIMBA 2007 experiment. Inbound track from Sep 24 to Sep 27; outbound track from Oct 24 to Oct 27; ICESat tracks (1) 1299 (Oct 4), (2) 0011 (Oct 8), (3) 0145 (Oct 17), (4) 0183 (Oct 20), (5) 0198 (Oct 21), and (6) 0302 (Oct 28); Tracks 2 and 3 are polar wards, Tracks 1, 4, 5, 6 are away from polar; S1, S2, S3 SIMBA ice stations; F, B, L, and P respectively SIMBA's Fabra site, Brussels site, Liege site, and Patria site.

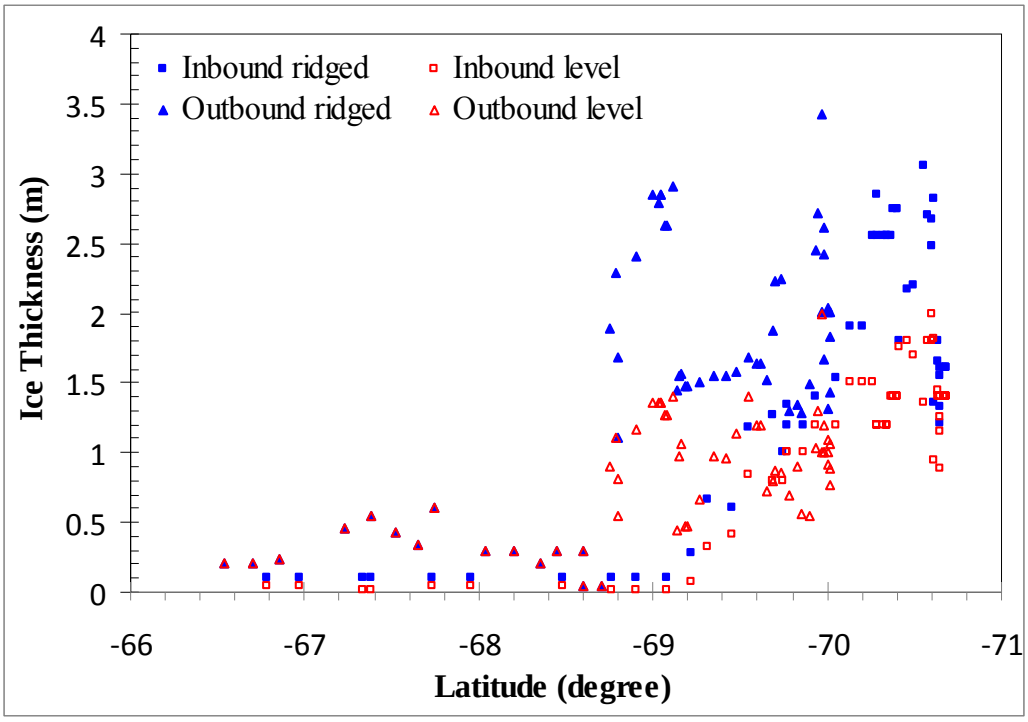

Figure 3. Observed ASPeCt ice thickness (red color denotes level ice only; blue color denotes all ices including ridges as calculated using equation 1) along inbound and outbound tracks (close to north-south) near the 90 W longitude.

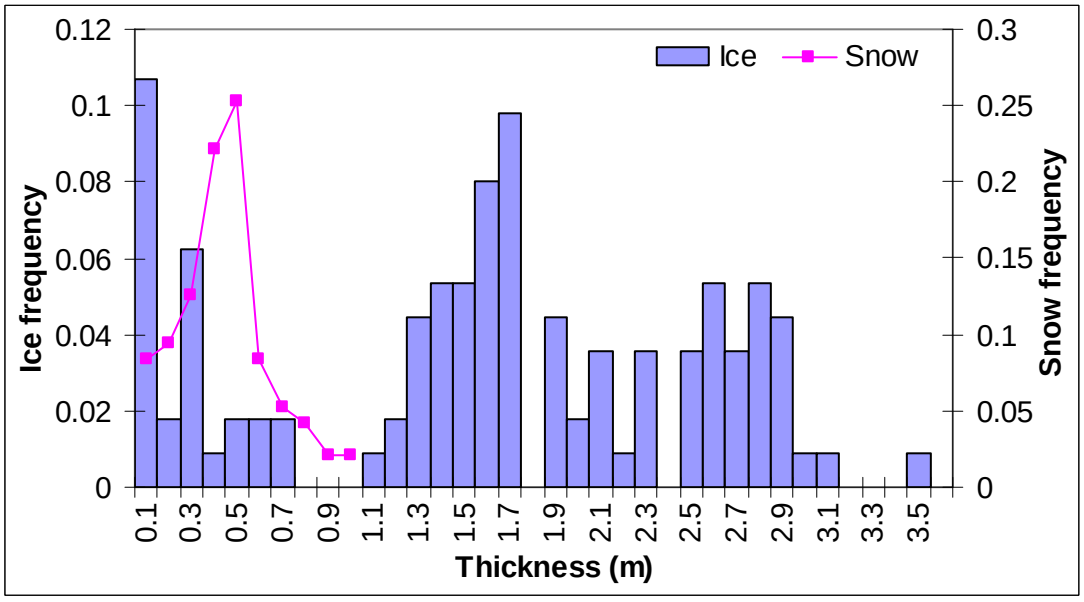

Figure 4. Distributions of total ASPeCt ice thickness and snow thickness along the inbound and outbound tracks

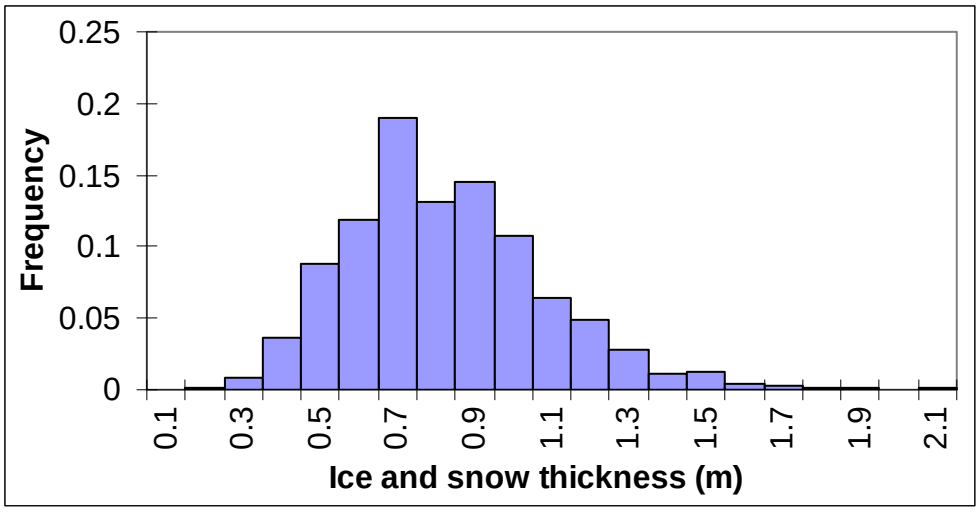

Figure 5. Cam 1 derived ice and snow thickness distribution for all photos (1296) from both inbound and outbound tracks.

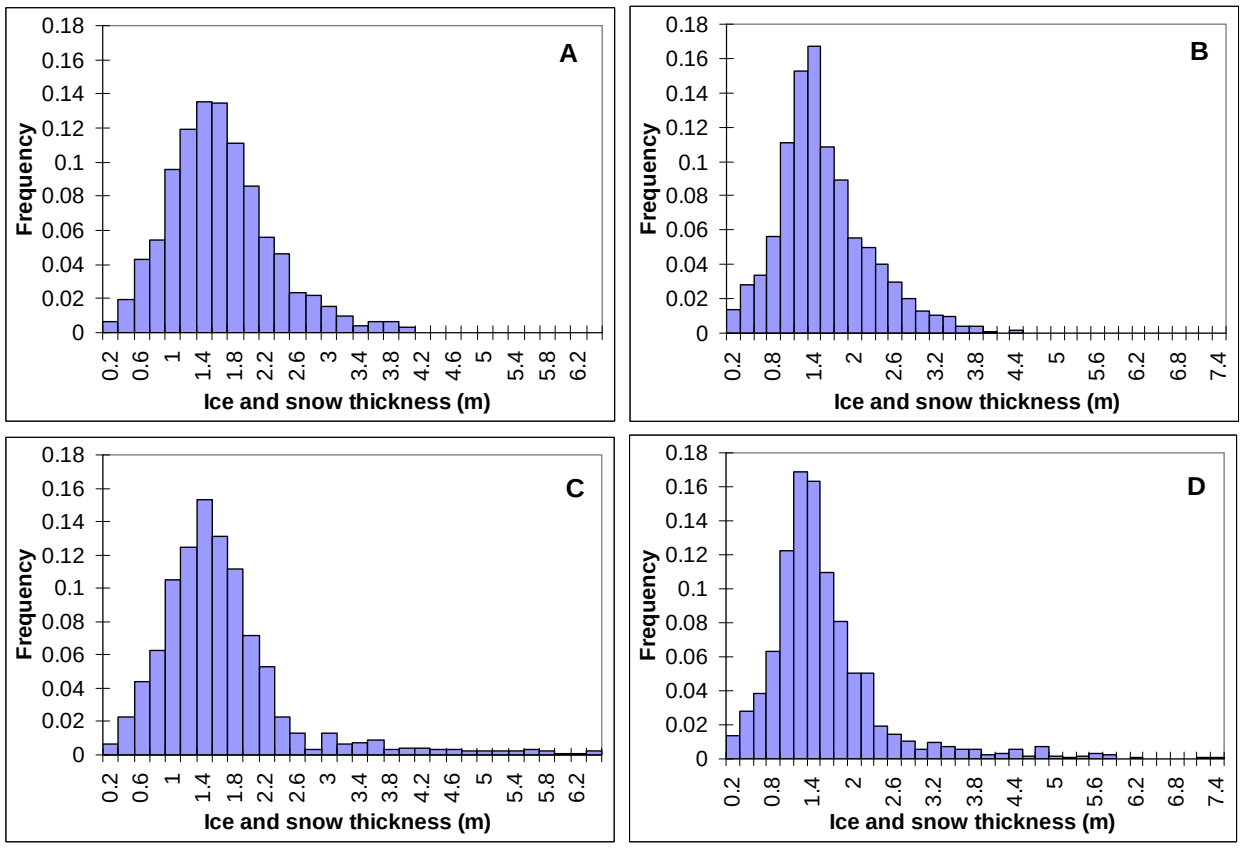

Figure 6. EM 31 estimated ice and snow thickness distribution for the inbound track (A, C) and outbound track (B, D). A, B are the original EM 31 thickness and C, D are the adjusted EM thickness using equations 2 and 3.

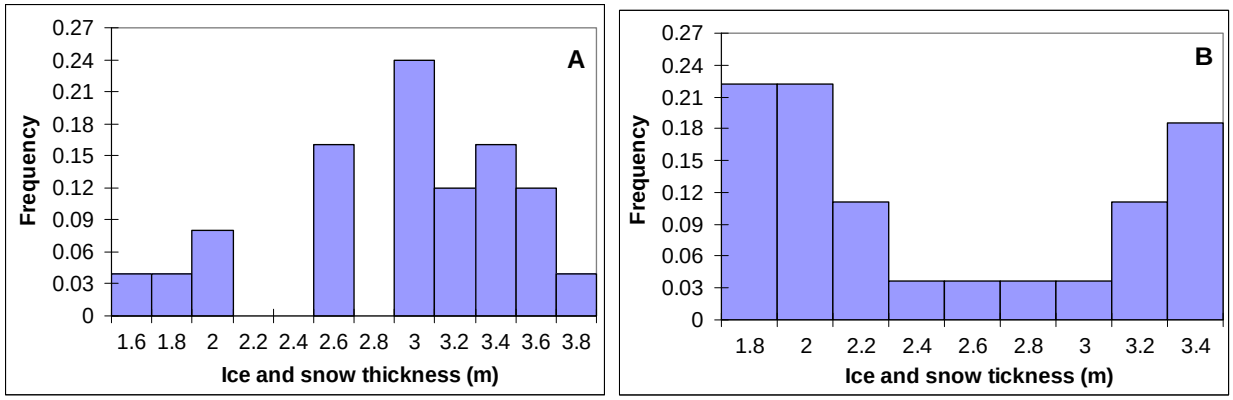

Figure 7. ASPeCt ice and snow thickness for the period when EM 31 were in operation for the inbound (A) and outbound (B) tracks.

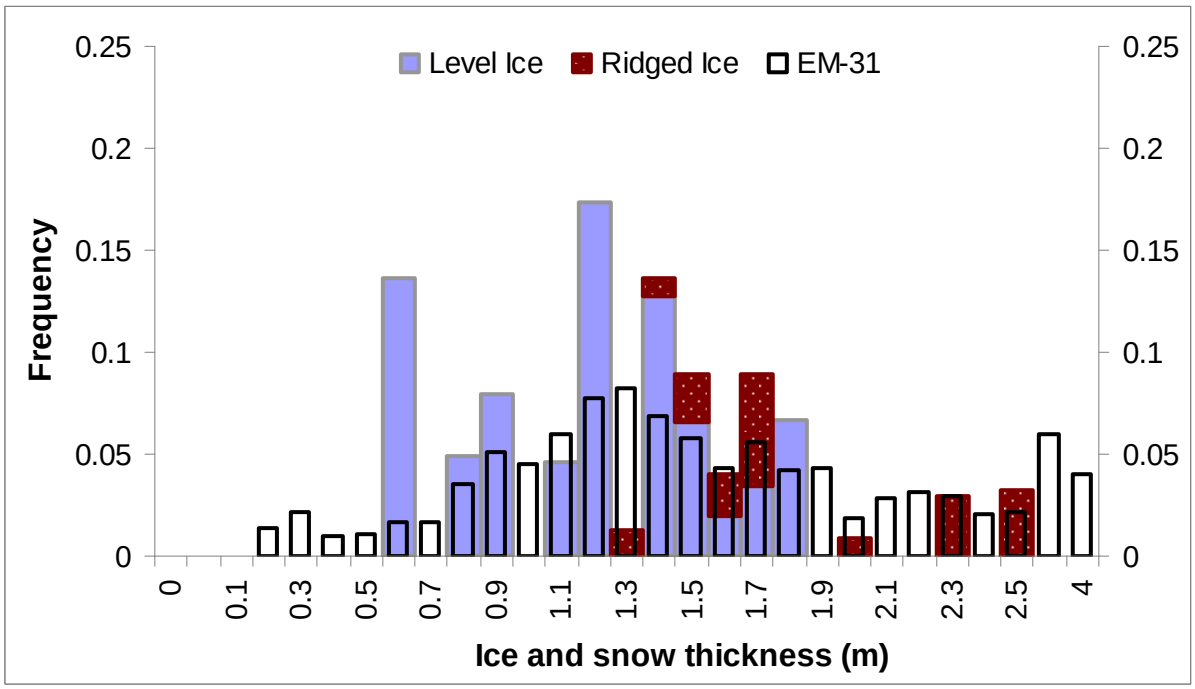

Figure 8. Frequency distribution of ASPeCt level and ridged ice thickness and EM 31 thickness for Oct 25, 2007.

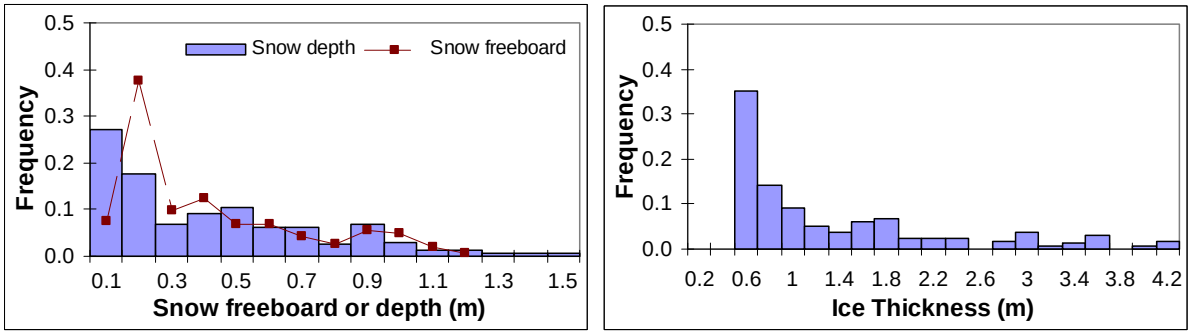

Figure 9. Frequency distributions of Snow depth and freeboard (left) and ice thickness (right) from the 163 in situ measurements at the five stations and sites during SIBMA 2007.

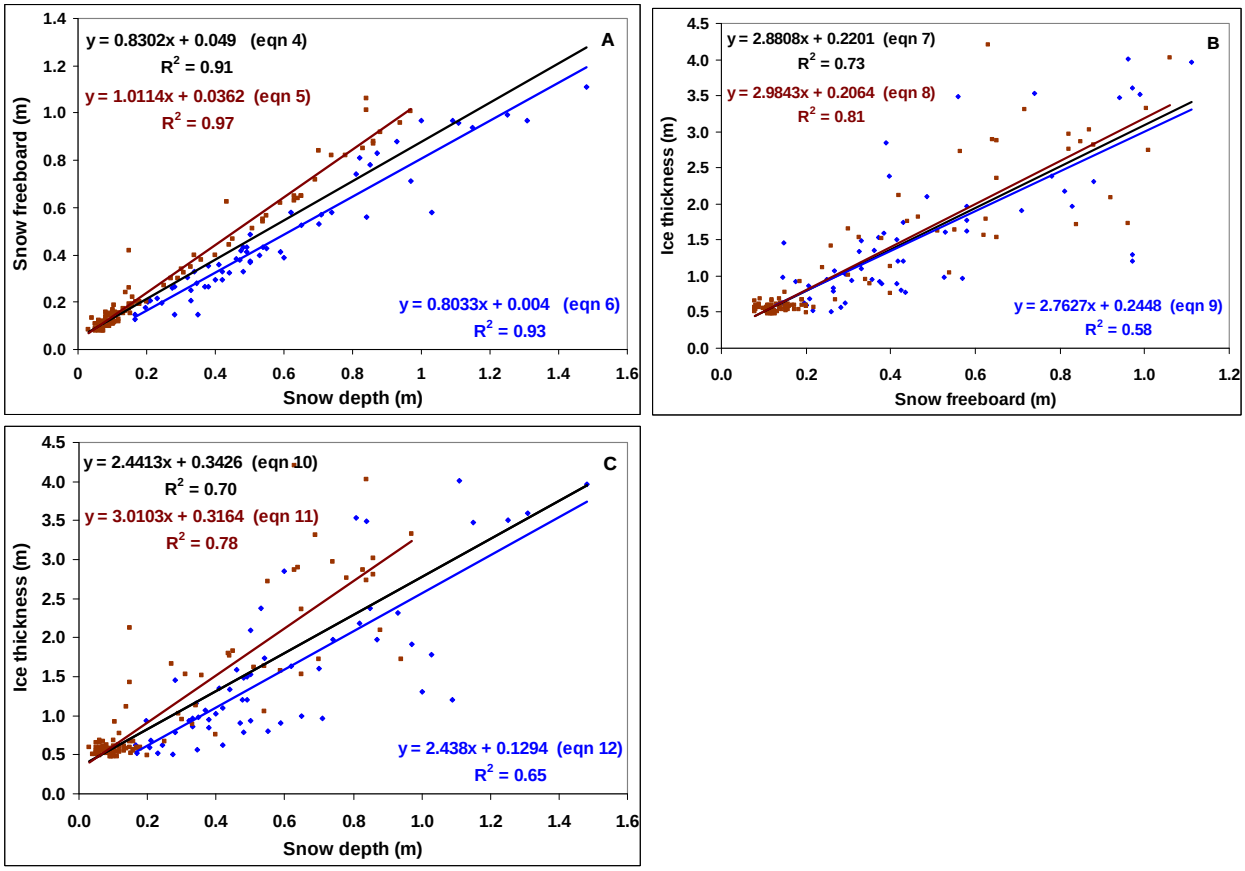

Figure 10. Scatter plots and correlations between Snow depth, snow freeboard, and ice thickness measurements from the SIMBA profiles. Black lines and black equations are from all samples, deep red dots and lines are from measurements (105) with ice freeboard >=0, blue dots and lines are from measurements (58) with negative ice freeboard.

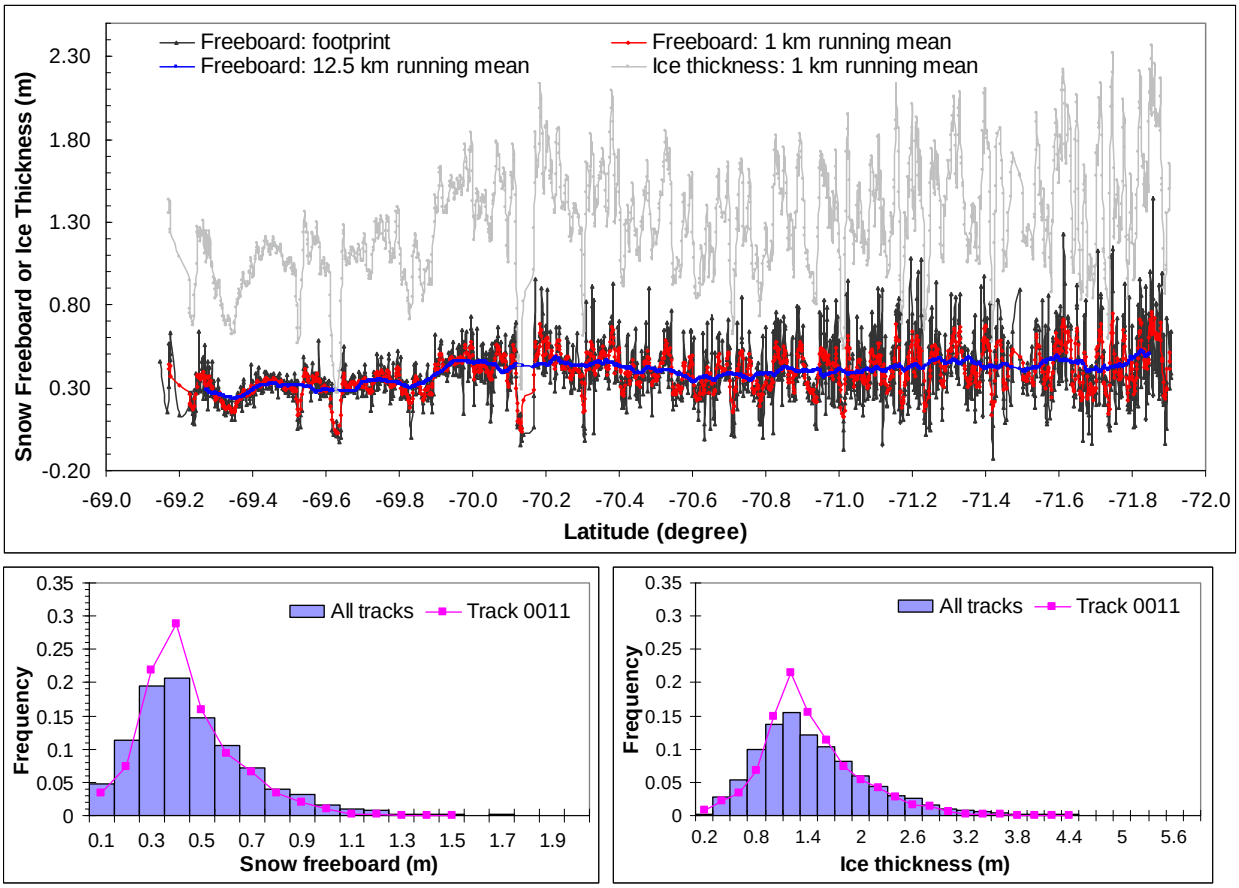

Figure 11. ICESat snow freeboard and ice thickness profile from track 0011 (Oct 8, 2007, top panel) and frequency distributions of snow freeboard for track 0011 and all tracks (bottom left) and ice thickness for track 0011 and all tracks (bottom right)

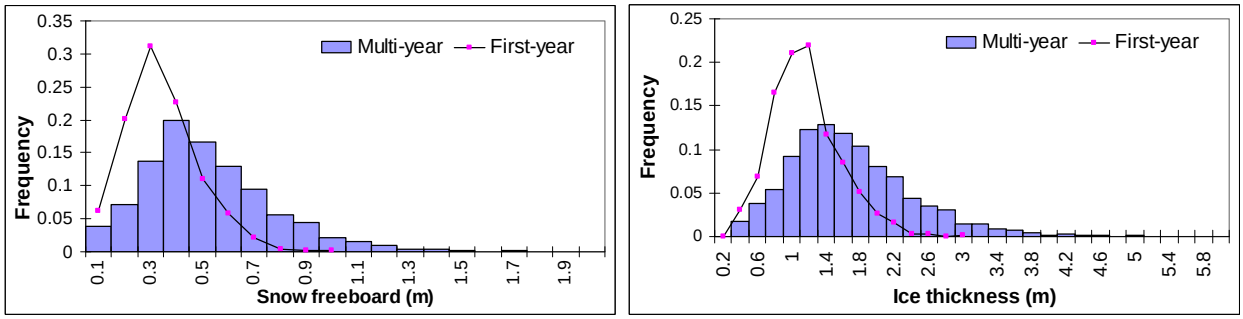

Figure 12. ICESat snow freeboard (left) and ice thickness (right) distributions for first year ice and multiyear ice from the six ICESat tracks.